ARTICLE

Analyzing the Effects of Tool Holder Stiffness on Chatter Vibration Reduction in Turning

Kadir Gok[1] , *Erol Turkes[2]* , *Özler Karakas[3]* , *Arif Gok[4*]*

[1] *Department of Biomedical Engineering, Engineering and Architecture Faculty, Izmir Bakircay University, Izmir, 35000, Turkey*

[2] *Department of Mechanical Engineering, Engineering Faculty, Kırklareli University, Kırklareli, 39010, Turkey*

[3] *Department of Mechanical Engineering, Engineering Faculty, Pamukkale University, Denizli, 20100, Turkey*

[4] *Department of Industrial Design, Architecture Faculty, Kutahya Dumlupinar University, Kutahya, 43020, Turkey*

ABSTRACT

This paper investigates the effects of tool holder materials on chatter vibration in turning operations. The study uses a complex dynamic turning model with two degrees of freedom for the orthogonal cutting system. Tool holders made from different materials, including Al 5083, Al 6082, Al 7012, and a standard 4140 material, were subjected to chatter vibration to investigate their process damping capabilities. The study found that the standard tool holder 4140 allows for higher stable depths of cut and produces similar process damping values compared to the other tool holders. Finite element analyses (FEA) were performed to verify the experimental results, and the modal and FEA analyses produced very similar results. The study concludes that future research should investigate the effects of tool holders made from high alloy steel alloys on process damping. Overall, this paper provides important insights into the effects of tool holder materials on chatter vibration and process damping in turning operations, which can help in the design of more efficient and effective cutting systems.

Keywords: Turning; Tool holder; Chatter; Process damping; Finite element analysis

1. Introduction

Process damping is a condition that it reduces chatter vibrations during cutting. It is estimated that process damping occurs due to plunging wavy work surface of cutting tool and instantaneous work surface slope (δ) generated by the tool oscillation [1]. Also, the process damping force is non-linear and the modeling process is still challenging, and although it is known why and how this force is generated, the fundamental issue is not fully understood. The reason for this is that the process damping force is nonlinear, and its fundamental properties are not fully understood. Until now, a mathematical model has not yet been developed to describe the relationship between the clearance angle and the process damping force, despite many investigations. Moreover, a mathematical equation that can be used to define this relation has not yet been fully presented. In addition, it is generally known that process damping, when seen at low speeds, is also important for average cutting speeds depending on the vibration frequency [2,3]. Research and experiments have indicated that process damping increases thanks to increase in attach the length of the cutting tool and a decrease in spindle speed. If so, the waves on the surface of workpiece become sharply pointed by wavelength decreasing according to $Lw = n \, [rpm]/\omega_c \, [Hz]$ equation [3,4]. Because of important structural features of cutting tool for chatter frequency, investigation of effects on process damping of cutting tool features (materials, dimensions, etc.) may be worthwhile.

This study employs a multidisciplinary approach to investigate the effects of tool holder materials on chatter vibration in turning. The use of analytical, experimental, and numerical methods allows the researchers to gain a more complete understanding of the mechanisms that contribute to chatter vibration and to identify effective strategies for reducing this type of vibration. The ultimate goal of this research is to improve the quality and efficiency of turning operations by reducing the negative effects of chatter vibration on the parts being machined.

2. Modeling of the cutting system

The dynamic cutting system was modeled by E. Turkes et al. [1]. The ratios of Process Damping Ratio (PDR) values calculated due to shear angle oscillations and penetration forces resulting from the contact of the wavy surface and the tool flank surface is determined. Scheme of dynamic cutting system was given in **Figure 1**.
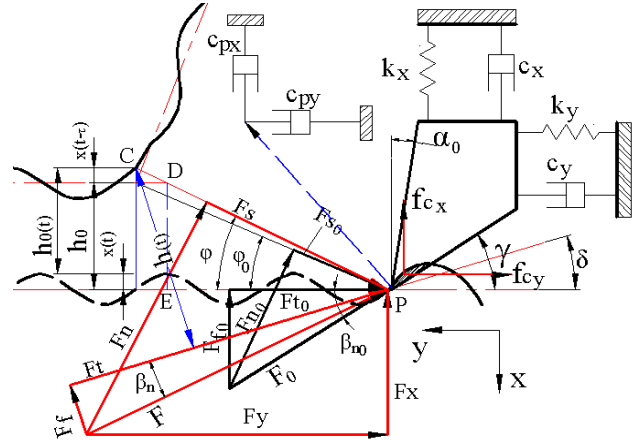

Figure 1. Dynamic cutting model [1].

According to **Figure 1**, the equations of motion of the cutting tool in the (x) and (y) directions, without considering penetration:

$$m_x \, \ddot{x}(t) + c_x \, \dot{x}(t) + k_x \, x(t) = F(t)\sin(\beta_n + \delta) = -F_{xTot}(t)$$
$$m_y \, \ddot{y}(t) + c_y \, \dot{y}(t) + k_y \, y(t) = F(t)\cos(\beta_n + \delta) = -F_{yTot}(t)$$
(1)

Total dynamic forces in both directions in **Figure 1** are expressed as:

$$F_{xTot}(t) = -\big(F_x(t) + f_{cx}(t)\big); \, F_{yTot}(t) = -\big(F_y(t) + f_{cy}(t)\big) \,\, (2)$$

where $f_{cx}(t)$ and $f_{cy}(t)$ are resistance force components in the (x) and (y) directions and they can be expressed as: $f_{cx}(t) = c_{px}\dot{x}(t); \, f_{cy}(t) = c_{py}\dot{y}(t)$. Equations of motion in both directions of the system by taking into account these forces can be arranged as follows:

$$m_x \, \ddot{x}(t) + c_x \, \dot{x}(t) + k_x \, x(t) = -F_x(t) - f_{cx}(t)$$
$$m_y \, \ddot{y}(t) + c_y \, \dot{y}(t) + k_y \, y(t) = -F_y(t) - f_{cy}(t)$$
(3)

The equations of motion in the (x) and (y) directions by substituting in Equation (3) expressions of the resistance force components are written as follows:

$$m_x \, \ddot{x}(t) + \left(c_x + c_{px}\right)\dot{x}(t) + k_x \, x(t) = -F_x(t)$$

$$m_y \, \ddot{y}(t) + \left(c_y + c_{py}\right)\dot{y}(t) + k_y \, y(t) = -F_y(t) \tag{4}$$

As indicated in Equation (4), if add the penetration damping ($C_{px,py}$) to the structure damping ($C_{x,y}$) the total damping is obtained $C_{tx} = C_x + C_{px}$; $C_{ty} = C_y + C_{py}$. Static and Dynamic Cutting Force Coefficients (DCFC) are written in Equation (4) and the equations of motion in the (x) and (y) directions are written as follows:

$$m_x \, \ddot{x}(t) + c_{tx} \, \dot{x}(t) + k_x \, x(t) =$$
$$-\tau_s \, a \, \lambda_{sx}\left(h_0 - x + x(t-\tau) + \lambda_{dx} \, \dot{x} - \lambda_{vx} \, \dot{y}\right)$$
$$m_y \, \ddot{y}(t) + c_{ty} \, \dot{y}(t) + k_y \, y(t) = \tag{5}$$
$$-\tau_s \, a \, \lambda_{sy}\left(h_0 - x + x(t-\tau) + \lambda_{dy} \, \dot{x} - \lambda_{vy} \, \dot{y}\right)$$

If the equation Equation (5) is arranged with τ-Decomposition method [5], as a result, it can be written as follows:

$$m_x \, \ddot{x}(t) + c_{tsx} \, \dot{x}(t) + k_x \, x(t) + c_{vy} \, \dot{y}(t) = F_{esx}\left(x(t) - x(t-\tau)\right)$$
$$m_y \, \ddot{y}(t) + c_{tsy} \, \dot{y}(t) + k_y \, y(t) + c_{dy} \, \dot{x}(t) = F_{esy}\left(x(t) - x(t-\tau)\right) \tag{6}$$

where (C_{tsx}) and (C_{tsy}) are the last total damping in both directions. According to a constant of the point (P) in **Figure 1**, $h_0 + x(t-\tau) = x(t-\tau)$ and $x(t) = x(t)$, where $c_{tsx} = c_{tx} + a \, K_f \, \lambda_{dx}$; $c_{tsy} = c_{ty} - a \, K_t \, \lambda_{vy}$; $c_{vy} = -a \, K_f \, \lambda_{vx}$; $c_{dy} = a \, K_t \, \lambda_{dy}$; $F_{esx} = -a \, K_f$; $F_{esy} = -a \, K_t$.

3. Experimental setup

CutPro 8 and the impact force hammer set and software are used for model analysis as seen in **Figure 2**. Material of workpiece was chosen as AISI-1010 ($K_f = 1 \times 10^{+9} N/m^2$). The cutting tool has cross-section dimensions of 20×20 mm. It was attached as L = 70-110 mm. The experimental model analysis of the cutting system was executed for measuring the transfer functions using a hammer tool with a force converter and an accelerometer fixed to the machine tool structure. An accelerometer was used to measure weights in the range ± 50 g, sensitive 104.3 mV/g, the resonant frequency is 40.0 kHz and an impact force hammer with a force range is 0-500 N, sensitivity is 10 mV/N impulse.
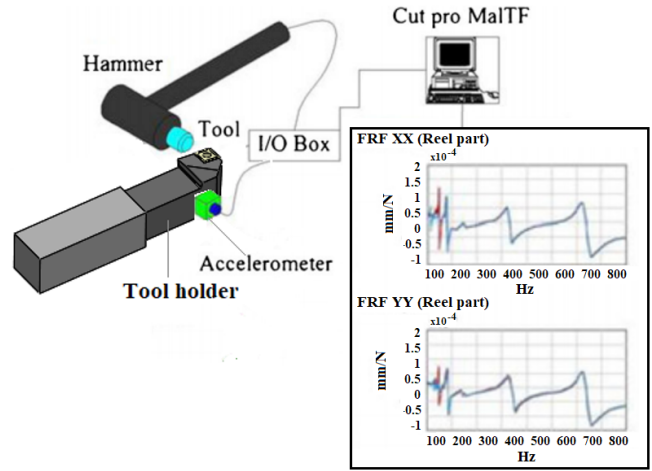

Figure 2. The experimental setup.

4. Computer aided analysis

Cutting processes are analytically complex and require advanced methods such as computational fluid dynamics (CFD) and finite element analysis (FEA) to accurately model and analyze the various physical phenomena involved. These methods allow researchers to simulate and analyze the behavior of cutting tools and workpieces under different load and boundary conditions, and to predict the performance of cutting systems under different operating conditions.

However, it is important to note that the accuracy of FEA and CFD simulations depends heavily on the quality of the input data and the assumptions made in defining the load and boundary conditions. Inaccurate or incomplete input data can lead to incorrect or unreliable results [6]. Therefore, careful attention should be paid to the modeling and simulation process to ensure that the results are accurate and reliable.

FEA and CFD have been used in a variety of applications, including metal turning, bone drilling, water jet cutting, and simulations of COVID-19 and other infections. In metal turning, for example, FEA can be used to predict the cutting forces, temperature distribution, and tool wear in a cutting process [6-17]. Analytical models can also be used to calculate cutting parameters, as demonstrated by Türkes et al. in their research [14].

It is common practice to use finite element-based software such as ANSYS Workbench to simulate the behavior of cutting tools and tool holders. The software allows researchers to create detailed 3D models of the cutting tool and tool holder and simulate the stresses and deflections that occur during the cutting process.

In this study, the deflections on the tool holder were predicted using ANSYS Workbench, which is a widely used software in the field of engineering for simulating and analyzing the behavior of complex systems. The 3D modeling of the cutting tool and tool holder was performed using SolidWorks, which is a popular CAD (computer-aided design) software in **Figure 3**.

Using these software tools, researchers can accurately predict the behavior of the cutting tool and tool holder under various load and boundary conditions, and optimize the design of the cutting system to reduce chatter vibration and improve the quality and efficiency of the machining process.

Finite element model

The 3D models send to the ANSYS workbench. The meshing process performs for FEA. The mesh structures of the models have been performed using the hexagonal element type as indicated in **Figure 4**. While the mesh size has been defined as 0.25 mm for insert and base, other components as 2 mm. The FEA model has 116205 nodes and 65732 elements. The cutting tool holder has been fixed from the support. The contact definitions between the support, tool holder, insert and base have been defined as a bounded contact. The mechanical properties of tool holders used in cutting tests have been in **Table 1**.
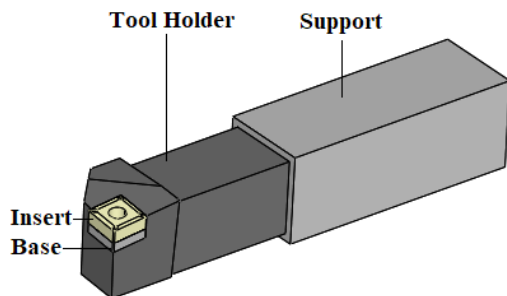
Figure 3. Cutting tool and holder.
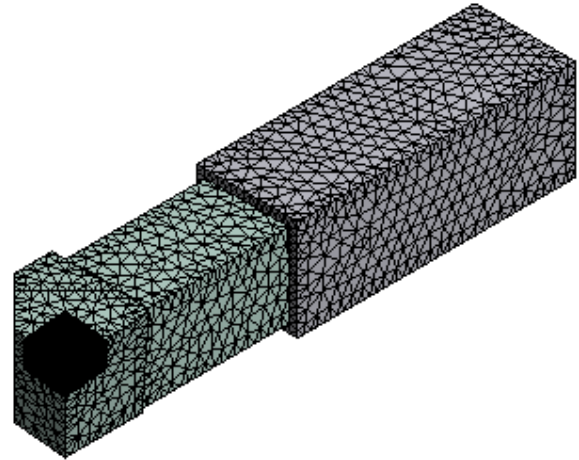
Figure 4. Mesh generation of the cutting tool system.

Table 1. The mechanical properties of tool holders.

Tool Holder Materials	Density	Young Modulus (GPa)	Poisson Ratio	Yield Strength (MPa)
Al-5083	2660	70.3	0.33	190
Al-6082	2680	70	0.33	240
Al-7012	2840	70	0.33	540
Stan-4140	7850	205	0.29	675

5. Results and discussions

The obtaining values were given in **Table 2** and the experimental results were indicated in **Figure 5** and **Figure 6** for the Al-5083 tool holder for an attach length of tool L = 70 mm. Modal analysis tests were performed for other tool holders at different fixing lengths and modal test results were obtained. The reason why tool holders made of different materials are attached at different fixing lengths for turning operations is to observe their effects on chatter vibration at high and low frequencies. **Figure 6** shows the chatter frequency image obtained at the stable cutting depth limit (a_{lim}), that is, at the border where chatter vibration begins to occur. Chatter frequencies ($\omega_c[Hz.]$) in **Table 2** have been acquired by LabView 7.1 software using cutting tests.

Chatter frequencies (ω_c [Hz.]) in **Table 2** were obtained using the LabView 7.1 software with cutting tests. For this, the noise generated by the cutting tool is recorded by a microphone and processed in LabView software.

Table 2. Results of tests.

| Tool holder Materials	Tool length L [mm]	Natur.frEquation ω_n [Hz]	Stiffness k [N/m]	Damp.ratio ζ [%]	Chatt.frEquation ω_c [Hz]
Al-5083	70	2312	8.44×10^6	1.27×10^{-2}	2650
	110	1047	2.43×10^6	5.57×10^{-3}	1150
Al-6082	70	2249	8.26×10^6	1.79×10^{-2}	2500
	110	1019	2.11×10^6	1.14×10^{-2}	1150
Al-7012	70	2349	8.98×10^6	1.45×10^{-2}	2750
	110	1104	2.38×10^6	5.95×10^{-3}	1220
Stan-4140	70	1511	1.22×10^7	2.92×10^{-2}	1820
	110	748	3.67×10^6	1.14×10^{-2}	930
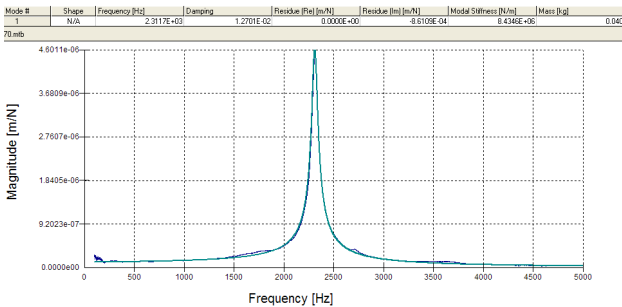
Figure 5. Modal analysis results for Al-5083 material and L = 70 mm.
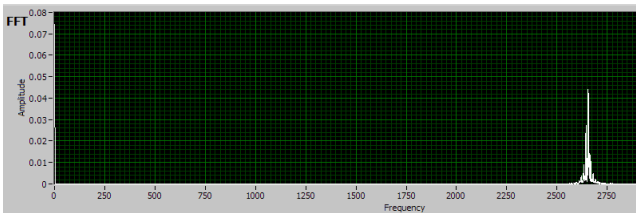
Figure 6. Microphone noise test result (ω_c) for Al-5083 material and L = 70 mm.

The boundaries of experimental and computationally stable axial cutting depths are indicated in **Figure 7**. This stability lobe diagram is plotted for attach length L = 70 of the tool holder with Al-5083 material. Where, calculational line is obtained by equations of process damping model. Critic line is obtained by traditional method. As can be seen from **Figure 7**, difference between calculational line and a critical line is increasing at low and medium spindle speeds. **Figure 8** shows stability lobe diagrams for Stan-4140 material and L = 70 mm. **Figure 9** shows time domain diagram for Al-5083 material and L = 70 mm. **Figure 10** shows time domain diagram for Stan-4140 material and L = 70 mm. **Figure 11** shows time domain force diagram for Al-5083 material and L = 70 mm. **Figure 12** shows time domain

force diagram for Stan-4140 material and L = 70 mm. **Table 2** shows outputs of the dynamic cutting model simulations.
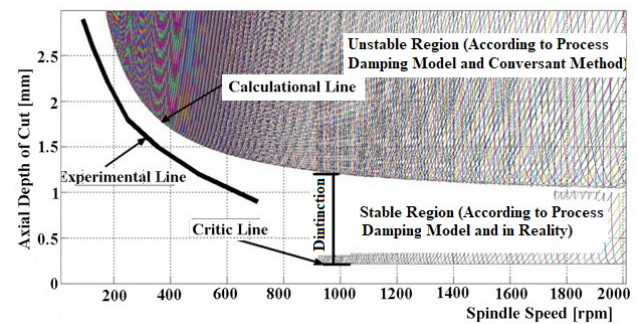

Figure 7. Stability lobe diagrams for Al-5083 material and L = 70 mm.
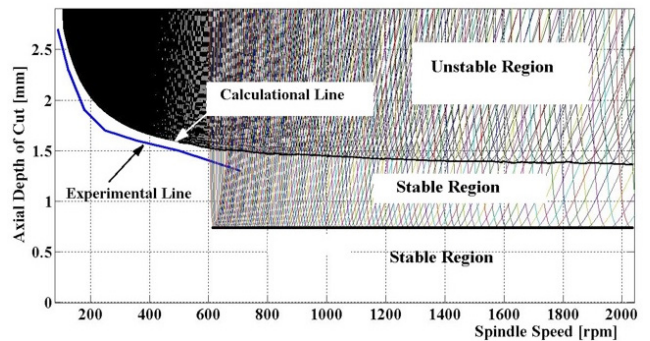

Figure 8. Stability lobe diagrams for Stan-4140 material and L = 70 mm.

By the time domain dynamic force analysis method for all tool holders, the changes of dynamic cutting forces were obtained as indicated in **Table 3**. Force values have been obtained to obtain how these tool holders are forced under dynamic cutting forces. These force values were obtained for cutting depths at the chatter vibration start limit. This limit is the stable depth of cut limit (a_{lim}).

Table 3. Outputs of the dynamic cutting model simulations.

Tool holder Materials	Tool length L [mm]	Amplitude [mm]	Stable Cutting Depth [mm]	Dynamic Resultant Cutting Force [N]	Dynamic Feed Force F_x [N]	Dynamic Tangential Force F_y [N]
Al-5083	70	1.1×10^{-2}	0.7	374.5……387.0	128.1….132.4	352…..363.7
	110	1.2×10^{-2}	0.1	70.7…….93.0	24.2….31.81	66.44…..87.4
Al-6082	70	1.7×10^{-2}	0.90	518.6……537.7	177.4….183.9	487.3…..505.3
	110	2.6×10^{-2}	0.25	147…….160	50.3…..80	138.2…..150.4
Al-7012	70	1.6×10^{-2}	0.77	456…….472	156….161.5	428.5….443.6
	110	3.2×10^{-2}	0.32	180.8…….199.2	61.9….68.2	170…..187.2
Stan-4140	70	2.4×10^{-2}	2.1	1245.3……1327.5	426…..454.1	1170.2...1247.5
	110	5.8×10^{-2}	0.5	373……..384	127.5….131.3	350.5…360.8

Table 3 also gives the amplitude values of the vibration of the tool dynamically cutting at stable depths of cut (a_{lim}). Vibration amplitude values were also obtained as a result of time domain simulations. **Figure 9** and **Figure 10** give examples of vibration amplitudes for tool holders made of Al-5083 and Standard-4140 materials for fixing lengths L = 70 mm.
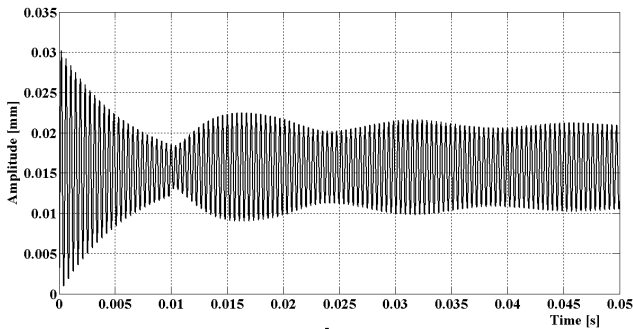

**Figure 9.** Time domain diagram for Al-5083 material and L = 70 mm.
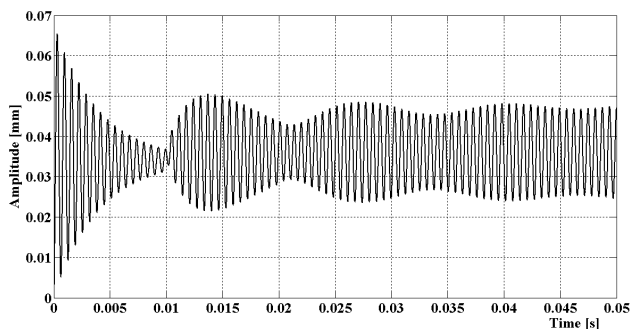
Figure 10. Time domain diagram for Stan-4140 material and L = 70 mm.

By means of time domain simulations, the shear force diagrams occurring at the limit of stable cutting depth (a_{lim}) were obtained as indicated in **Figure 11** and **Figure 12**. The maximum and minimum dynamic shear forces eliminated from these diagrams are given in **Table 3**. From the time domain simulations used, the values of the components of the dynamic cutting forces (F_x) and (F_y) in the direction of advance (x) and the tangential direction (y) of the cutting tool were also obtained and are indicated in **Table 3**. Using all these dynamic force values obtained, finite element analysis has been made for tool holders with all different materials. As a result of this analysis, the stress zones and stress values of the tool holders were obtained. During the dynamic cutting experiments of tool holders, FEA analysis was performed for two different insertion lengths attached to the machine tool.
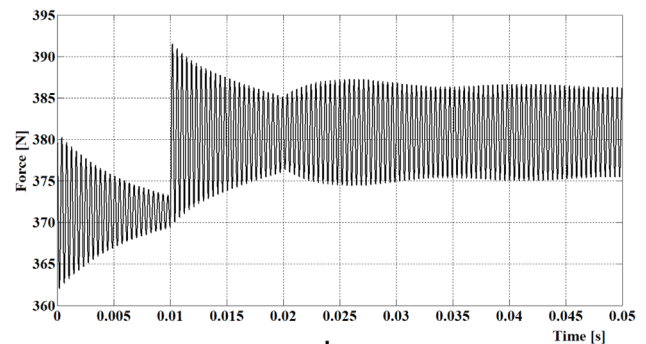
Figure 11. Time domain force diagram for Al-5083 material and L = 70 mm.
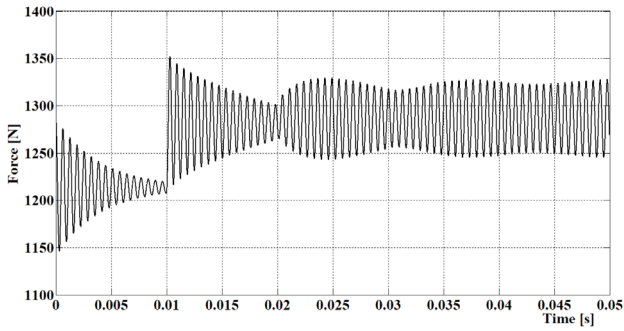
Figure 12. Time domain force diagram for Stan-4140 material and L = 70 mm.

As a result of FEA, stress and deflections of the tool holder was given in **Table 4**. For four different materials, deflections the tool holder was calculated very close to each other. It was also given the deflections in **Figure 13**.

Table 4. Tool holder stress and deformations.

Tool Holder Materials	von-Mises Stress (MPa)	Deflection (mm)	Young Modulus (GPa)	Yield Strength (MPa)
Al-5083	23.63	0.026	70.3	190
Al-6082	32.82	0.037	70	240
Al-7012	28.81	0.032	70	540
Stan-4140	86.54	0.033	205	675
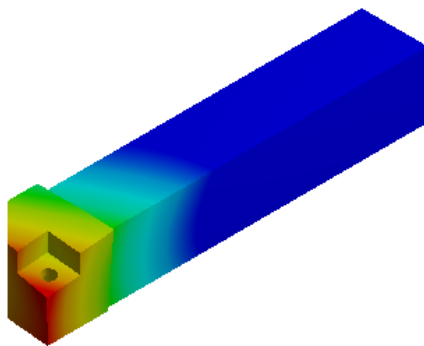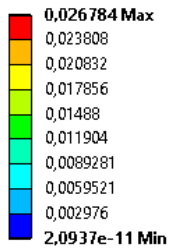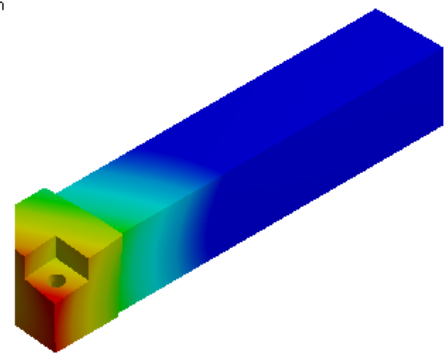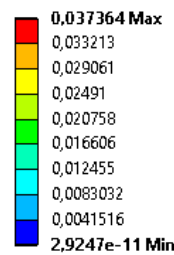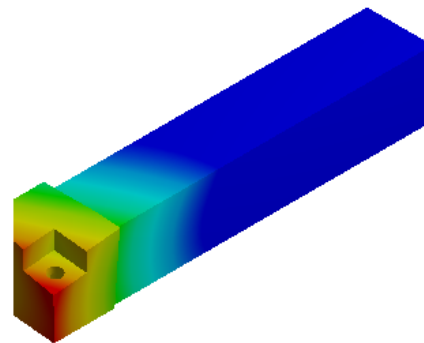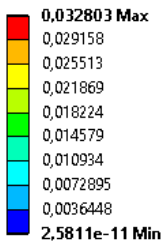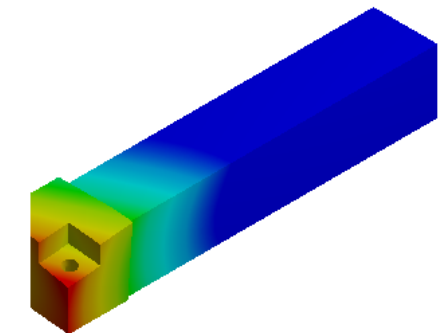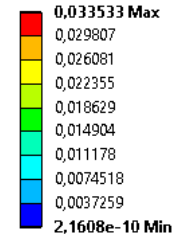
Figure 13. The deflections in different material having tool holder: a) Al-5083, b) Al-6082, c) Al-7012, d) Stan-4140.

6. Conclusions

In this study, tool holders with different materials such as Al 5083, Al 6082, Al 7012 and standard 4140 that are oscillated by chatter vibration are used to investigate the process damping of the cutting system. First, a mathematical model for dynamic cutting is obtained. The mathematical model of dynamic shear is considered as two degrees of freedom. This model has been created by considering the variation of the shear angle (φ) caused by the deflection (δ) of the cutting tool and the penetration of the cutting tool into the undulating surface formed on the cut surface of the workpiece in the previous period. The main purpose was to investigate the effects of tool holders made of different materials on process damping caused by chatter vibration. Afterward, modal analysis tests, stable shear tests and dynamic shear tests were performed to obtain some values required for the obtained complex mathematical model. It has been observed from the dynamic cutting tests that the stable cutting depth (a_{lim}) gradually increases as the tool holder material hardens and its strength increases. In dynamic cutting tests, stable cutting depths (a_{lim}) were obtained by gradually increasing the depths of cut. The depth of cut at which the chatter vibration started was recorded as a stable depth of cut. Chatter vibration started with the microphone test and it was determined when the chatter sound was recorded and a chatter frequency (ω_c) close to the natural frequency was obtained. When the values obtained from all tests are applied to the simulation written in the Matlab code, the stability lobe diagrams (SLD) obtained with the process damping (traditional chatter analysis method) and the developed process damping method are drawn. As can be seen from these SLDs, it has been observed that there is no difference in terms of process damping between the standard tool holder and the tool holder made of different materials. It has even been found that higher stable depths of cut can be completed with the standard tool holder. It is anticipated that the process damping values that can be obtained may be similar. It has been verified by FEA. The very close results have been obtained in modal and FEA analyses. It has been concluded that it may be useful to investigate the effects of tool holders to be manufactured from high alloy steel alloys on process damping for future studies on this subject.

Conflict of Interest

On behalf of all authors, the corresponding author states that there is no conflict of interest.

Acknowledgement

References

[1] Turkes, E., Orak, S., Neseli, S., et al., 2011. A new process damping model for chatter vibration. Measurement. 44, 1342-1348.

[2] Turkes, E., Orak, S., Neseli, S., et al., 2012. Decomposition of process damping ratios and verification of process damping model for chatter vibration. Measurement. 45, 1380-1386.

[3] Altintas, Y., Eynian, M., Onozuka, H., 2008. Identification of dynamic cutting force coefficients and chatter stability with process damping. CIRP Annals. 57, 371-374.

[4] Tlusty, J., Tlusty, G., 2000. Manufacturing processes and equipment. Upper Saddle River. Prentice Hall: USA. Available from: https://books.google.com.tr/books?id=xTBvQgAA-CAAJ.

[5] Turkes, E., Orak, S., Neseli, S., et al., 2011. Linear analysis of chatter vibration and stability for orthogonal cutting in turning. International Journal of Refractory Metals and Hard Materials. 29, 163-169.

[6] Gok, K., 2015. Development of three-dimensional finite element model to calculate the turning processing parameters in turning operations. Measurement. 75, 57-68.

[7] Gok, A., Gok, K., Bilgin, M.B., 2015. Three-dimensional finite element model of the drilling

process used for fixation of Salter–Harris type-3 fractures by using a K-wire. Mechanical Sciences. 6, 147-154.

[8] Gok, K., Inal, S., 2015. Biomechanical comparison using finite element analysis of different screw configurations in the fixation of femoral neck fractures. Mechanical Sciences. 6, 173-179.

[9] Erdem, M., Gok, K., Gokce, B., et al., 2017. Numerical analysis of temperature, screwing moment and thrust force using finite element method in bone screwing process. Journal of Mechanics in Medicine and Biology. 17, 1750016.

[10] Gok, K., Inal, S., Gok, A., et al., 2017. Biomechanical effects of three different configurations in Salter Harris type 3 distal femoral epiphyseal fractures. Journal of the Brazilian Society of Mechanical Sciences and Engineering. 39, 1069-1077.

[11] Inal, S., Gok, K., Gok, A., et al., 2018. Should we really compress the fracture line in the treatment of Salter–Harris type 4 distal femoral fractures? A biomechanical study. Journal of the Brazilian Society of Mechanical Sciences and Engineering. 40, 528.

[12] Gok, K., Inal, S., Urtekin, L., et al., 2019. Biomechanical performance using finite element analysis of different screw materials in the parallel screw fixation of Salter–Harris Type 4 fractures. Journal of the Brazilian Society of Mechanical Sciences and Engineering. 41, 143.

[13] Pirhan, Y., Gok, K., Gok, A., 2020. Comparison of two different bowel anastomosis types using finite volume method. Computer Methods in Biomechanics and Biomedical Engineering. 23, 323-331.

[14] Türkes, E., Erdem, M., Gok, K., et al., 2020. Development of a new model for determine of cutting parameters in metal drilling processes. Journal of the Brazilian Society of Mechanical Sciences and Engineering. 42, 169.

[15] Ada, H.D., Erdem, M., Gok, K., 2021. Computational fluid dynamics simulation of erosion-corrosion in abrasive water jet machining. Surface Review and Letters. 28, 2150031.

[16] Gok, K., Selçuk, A.B., Gok, A., 2021. Computer-aided simulation using finite element analysis of protect against to coronavirus (COVID-19) of custom-made new mask design. Transactions of the Indian Institute of Metals. 74(5), 1029-1033.

[17] Gok, K., 2021. Investigation using finite element analysis of effect on crater geometry of different abrasive types in abrasive water jet machining. Surface Review and Letters. 28(7), 1-6.